Structures of lipid–DNA complexes: supramolecular assembly and gene delivery

Cyrus R Safinya

Recently, there has been a flurry of experimental work on understanding the supramolecular assemblies that are formed when cationic liposomes (CLs) are mixed with DNA. From a biomedical point of view, CLs (vesicles) are empirically known to be carriers of genes (sections of DNA) in nonviral gene delivery applications. Although viral-based carriers of DNA are presently the most common method of gene delivery, nonviral synthetic methods are rapidly emerging as alternative carriers, because of their ease of production and nonimmunogenicity (viral carriers very often evoke an undesirable and potentially lethal immune response). At the moment, cationic-lipid-based carriers have emerged as the most popular nonviral method to deliver genes in therapeutic applications, for example, CL carriers are used extensively in clinical trials worldwide. However, because the mechanism of transfection (the transfer of DNA into cells by CL carriers, followed by expression) of CL–DNA complexes remains largely unknown, the measured efficiencies are, at present, very low. The low transfection efficiencies of current nonviral gene delivery methods are the result of poorly understood transfection-related mechanisms at the molecular and self-assembled levels. Recently, work has been carried out on determining the supramolecular structures of CL–DNA complexes by the quantitative technique of synchrotron X-ray diffraction. When DNA is mixed with CLs (composed of mixtures of cationic DOTAP and neutral DOPC lipids), the resulting CL–DNA complex consists of a multilamellar structure (L_{α}^{C}) comprising DNA monolayers sandwiched between lipid bilayers. The existence of a different columnar inverted hexagonal (H_{II}^{C}) phase in CL–DNA complexes was also demonstrated using synchrotron X-ray diffraction. Ongoing functional studies and optical imaging of cells are expected to clarify the relationship between the supramolecular structures of CL–DNA complexes and transfection efficiency.

Addresses
Materials Department, Physics Department and Biomolecular Science and Engineering Program, University of California, Santa Barbara, CA 93106, USA;
e-mail: safinya@mrl.ucsb.edu

Current Opinion in Structural Biology 2001, 11:440–448

0959-440X/01/$ – see front matter

Abbreviations

AFM	atomic force microscopy
bp	base pair
CL	cationic liposome
DOPC	di-oleoyl phosphatidylcholine
DOPE	di-oleoyl phosphatidylethanolamine
DOTAP	di-oleoyl trimethylammonium propane
HAC	human artificial chromosome
SAXS	small-angle X-ray scattering
XRD	X-ray diffraction

Introduction

The entire field of gene therapy based on nonviral synthetic delivery systems has recently undergone a renaissance [1,2••,3,4] since the initial landmark studies by Felgner *et al.* [5] and Li and Huang [1]. This work was soon to be followed by numerous groups demonstrating gene expression *in vivo* in targeted organs [6,7] and by human clinical trials [8,3]. Felgner *et al.* [5] discovered that cationic liposomes (CLs), closed bilayer membrane shells of lipid molecules, when mixed with DNA to form CL–DNA complexes with an overall positive charge, enhance transfection (i.e. the transfer of DNA into cells followed by expression). They hypothesized that this was because CL–DNA complexes adsorbed more effectively to the anionic plasma membrane of mammalian cells via electrostatic interactions. Compared with other nonviral delivery systems, including anionic liposomes that encapsulate nucleic acid and the use of polycationic reagents such as polylysine, CLs tend to mediate a higher level of transfection in the majority of cell lines studied to date. Some of the advantages of using nonviral vectors for gene delivery are the absence of viral genes to cause disease and the nonimmunogenicity of synthetic carriers due to a lack of exposed proteins.

Without doubt, one of the principal and most exciting advantages of synthetic over viral methods of gene delivery is the potential to transfer and express (transfect) large pieces of DNA into cells. The proof of this concept was clearly demonstrated when partial sections of first-generation human artificial chromosomes (HACs) of order 1 Mbp were transferred into cells with CLs, although extremely inefficiently [9,10•]. The future development of HAC vectors will be extremely important for gene therapy applications; because of their very large size, HAC vectors would have the ability to deliver not only entire human genes (in many cases exceeding 100 kbp), but also their regulatory sequences, which are needed for the spatial and temporal regulation of expression. Viral vectors have a maximum gene-carrying capacity of 40 kbp [11].

Aside from the medical and biotechnological ramifications for gene therapy and gene and drug therapeutics, research on CL–DNA complexes should also shed light on other problems in biology. The development of efficient HAC vectors in the future, which will most probably occur once efficient synthetic nonviral delivery systems have been developed, is a long-range goal of studies designed to characterize chromosome structure and function. Furthermore, molecular biology studies would benefit substantially from the ability to transfect hard-to-transfect cell lines using synthetic delivery systems, for example, in

studies designed to characterize the structure of promoters of human genes in the appropriate cell lines.

Although the transfection efficiency of CL–DNA complexes is enhanced compared with traditional nonviral delivery systems, the mechanisms of transfection via cationic lipids remain poorly understood and are actively being investigated. At present, hundreds of plasmid DNA molecules are required for successful gene transfer and expression. The enhancement of transfection efficiencies using nonviral methods requires a full understanding of the supramolecular structures of CL–DNA complexes and their interactions with cell membranes, and of events leading to the release of DNA in the cytoplasm for delivery within the nucleus. We are now beginning to understand the precise nature of the supramolecular structures of CL–DNA complexes in different lipid membrane systems [12–17]. The transfection efficiencies of nonviral delivery methods may be improved through insights into transfection-related mechanisms at the molecular and self-assembled levels.

DNA chains dissolved in solution are known to give rise to a rich variety of condensed and liquid-crystalline phases. Studies show regular condensed DNA morphologies induced by multivalent cations [18] and liquid-crystalline phases at high concentrations of DNA [19]. More recently, there has been a flurry of experimental and theoretical work on DNA chains mixed with CLs. Oligolamellar structures had been reported in cryo-transmission electron microscopy studies by Gustafsson *et al.* [20]. A freeze-fracture electron microscopy study by Sternberg *et al.* [21] had also observed isolated DNA chains coated with a lipid bilayer. As I describe in this review, one of the more commonly occurring supramolecular assemblies, which forms spontaneously when DNA is complexed with CLs, is a multilayer assembly of DNA sandwiched between bilayer membranes, as shown schematically in Figure 1 [12–15,17].

Soon after the initial experimental reports on the supramolecular structures of CL–DNA complexes [12,17], a series of theoretical papers investigated the structure and thermodynamic stability of these complexes [22–28]. Analytical and numerical studies of DNA–DNA interactions occurring between membranes show the existence of a novel long-range repulsive electrostatic interaction [24–26]. Theoretical work on CL–DNA complexes has also led to the realization of a variety of novel new phases of matter in DNA–lipid complexes [27,28]. In particular, a novel new 'sliding columnar phase', which remains to be discovered experimentally, is predicted, in which the positional coherence between DNA molecules in adjacent layers is lost without destroying the orientational coherence of the chains from layer to layer. This new phase would be a remarkable new phase of matter if it exists and shares many fascinating similarities with flux lattices in superconductors.

Figure 1

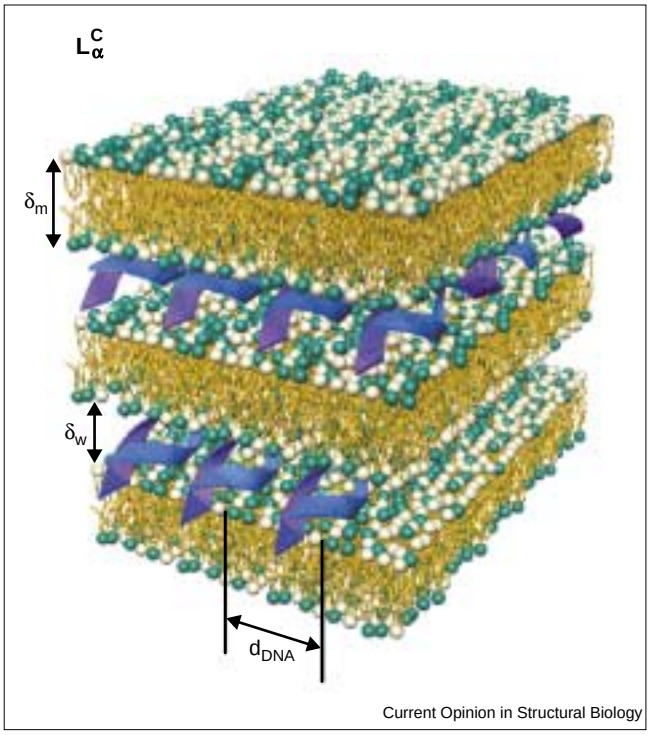

Schematic of the lamellar L_α^C phase of CL–DNA complexes, with alternating lipid bilayers and DNA monolayers. The DNA interaxial spacing is d_{DNA}. The interlayer spacing is $d = \delta_w + \delta_m$.

The lamellar L_α^C phase of CL–DNA complexes

A recent synchrotron X-ray diffraction (XRD) study of CL–DNA complexes [12,13] has revealed that the structure is different from the hypothesized 'bead-on-string' structure originally proposed by Felgner *et al.* [5] in their seminal paper, which pictured the DNA strand decorated with distinctly attached CLs. The addition of linear λ-phage DNA (48,502 bp, contour length = 16.5 μm) to binary mixtures of CLs (mean diameter = 70 nm), consisting of mixtures of neutral (so-called 'helper-lipid') DOPC (di-oleoyl phosphatidylcholine) and cationic DOTAP (di-oleoyl trimethylammonium propane), induces a topological transition from liposomes to collapsed condensates in the form of optically birefringent liquid-crystalline globules (on the order of 1 μm). Double-fluorescent microscopy of labeled DNA and lipid also shows the colocalization of lipid and DNA within the globules [12]. Polarized microscopy shows that the distinct globules are birefringent, indicative of their liquid-crystalline nature.

The precise structural nature of the CL–DNA complexes was elucidated by high-resolution synchrotron small-angle X-ray scattering (SAXS) experiments carried out at the Stanford Synchrotron Radiation Laboratory [12,13]. Figure 2 shows SAXS scans of dilute DOPC/DOTAP–λ-DNA mixtures at the isoelectric point of the complex (at which the cationic charge of DOTAP is equal to the anionic

Figure 2

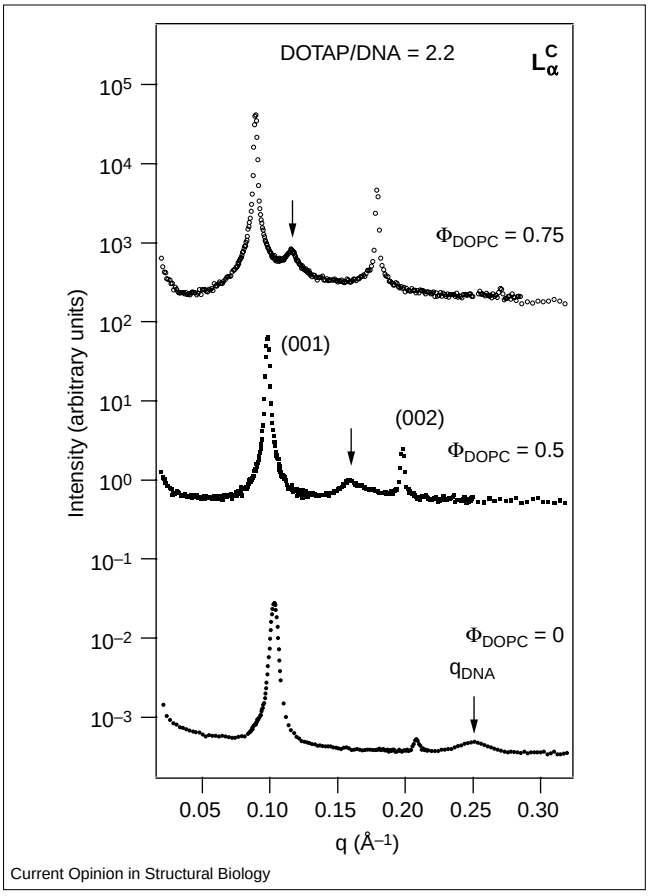

SAXS scans of CL–DNA complexes at constant DOTAP/DNA = 2.2 (at the isoelectric point) with increasing DOPC/DOTAP, which shows the DNA peak (arrow) moving towards smaller values of q as L/D (and Φ_{DOPC}) increases. Adapted from [12–14].

charge of DNA). In these experiments, the total lipid concentration (L = DOTAP + DOPC) was increased between lipid/DNA ratios (L/D) from 2.2 to 8.8 (wt/wt) at the isoelectric point (DOTAP/DNA = 2.20). Equivalently, the weight fraction of DOPC (Φ_{DOPC}) in the DOPC/DOTAP CL mixtures increased from 0 to 0.75. We see in Figure 2 that, at Φ_{DOPC} = 0.5 (L/D = 4.4), two sharp peaks are evident at q = 0.099 and 0.198 Å^{-1}, which correspond to the (00L) peaks of a layered structure with an interlayer spacing d (d = δ_m + δ_w) in the range 64 Å. The membrane thickness and water gap are denoted by δ_m and δ_w, respectively (Figure 1). The middle broad peak, q_{DNA}, arises from diffraction from the 1D lattice of DNA chains sandwiched between the lipid bilayers (Figure 1) and gives $d_{DNA} = 2\pi/q_{DNA}$= 39 Å, where d_{DNA} is the DNA interaxial spacing. Thus, the SAXS data lead to a model in which the CLs and DNA condense into a multilayer structure, denoted L_α^C, with DNA sandwiched between the bilayers (Figure 1).

In the absence of DNA, the lamellar L_α phase of membranes comprising DOPC and cationic DOTAP (1:1) exhibits strong long-range interlayer electrostatic repulsions that overwhelm the van der Waals attraction [29,30]. The interlayer spacing d is given by the simple geometric relation $d = \delta_m/(1-\Phi_w)$ (Φ_w is the volume fraction of water). From $d = 2\pi/q_{00L}$ at a given Φ_w, we obtain δ_m = 39 ± 0.5 Å for membranes with Φ_{DOPC} = 0.5. The DNA that condenses on the CLs screens the electrostatic interaction between lipid bilayers and leads to condensed multilayers. The average thickness of the water gap ($\delta_w = d-\delta_m$ = 64 Å – 39 Å = 26 Å) is just sufficient to accommodate one monolayer of B-DNA (diameter ≈ 20 Å), including a hydration shell consistent with Figure 1.

The SAXS scans in Figure 2 (arrow points to the DNA peak) show that d_{DNA} (= $2\pi/q_{DNA}$) increases with lipid dilution from 24.54 Å to 57.1 Å as the membrane charge density decreases with increasing Φ_{DOPC} between 0 and 0.75 (or, equivalently, increasing L/D between 2.2 and 8.8). The most compressed interaxial spacing of 24.55 Å at Φ_{DOPC} = 0 reflects the short-range repulsive hard-core interaction of the B-DNA rods containing a hydration layer [31]. Figure 3a plots d and d_{DNA} as a function of L/D. The observed behavior is depicted schematically in Figure 3b, showing that, as we add neutral lipid and lower the membrane charge density, at the isoelectric point the DNA chains also decrease their negative charge density by increasing the DNA interchain spacing. The solid line in Figure 3a is derived from the simple geometric packing relationship $d_{DNA} = (A_D/\delta_m)(\rho_D/\rho_L)$ (L/D), which equates the cationic charge density (due to the mixture $DOTAP^+$ and DOPC) with the anionic charge density (due to DNA^-). Here, ρ_D = 1.7 (g/cc) and ρ_L = 1.07 (g/cc) denote the densities of DNA and lipid, respectively, δ_m is the membrane thickness and A_D is the DNA area — $A_D = wt(\lambda)/[\rho_D L(\lambda)]$ = 186 Å^2, where wt(λ) is the weight of λ-DNA = 31.5*10^6/(6.022*10^{23}) g and L(λ) is the contour length of λ-DNA = 48502*3.4 Å.

The agreement between the packing relationship (solid line) and the data over the measured interaxial distance from 24.5 to 57.1 Å (Figure 3a) is quite remarkable given the fact that there are no adjustable parameters. The variation in the interlayer spacing ($d = \delta_w + \delta_m$) (Figure 3a, open squares) arises from the increase in the membrane bilayer thickness (δ_m) as L/D increases (each DOPC molecule is about 4–6 Å longer than a DOTAP molecule). The observation of a variation in the DNA interaxial distance as a function of the L/D ratio in multilayers (Figure 3a) unambiguously demonstrates that XRD directly probes the DNA behavior in multilayer assemblies. From the line widths of the DNA peaks (Figure 2), the 1D lattice of DNA chains is found to consist of domains extending to near 10 neighboring chains [13,15]. This is consistent with observations [32,33] by atomic force microscopy (AFM) imaging of DNA adsorbed on a cationic solid lipid bilayer supported on freshly cleaved mica surfaces (Figure 4). The success of these AFM preparations is in the direct observation of the periodic helical modulation of the double-stranded DNA molecules,

Figure 3

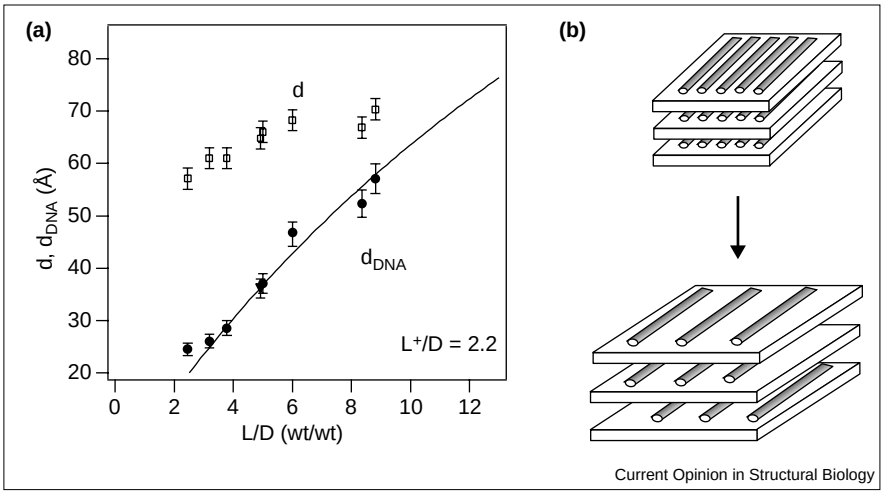

Data showing that the interaxial distance between DNA chains in the lamellar L_α^C complexes is controlled by the membrane charge density. **(a)** The DNA interaxial distance, d_{DNA} (closed circles), and the interlayer distance, d (open squares), in the L_α^C phase (Figure 2) plotted as a function of the L/D (wt/wt) ratio at the isoelectric point of the complex, DOTAP/DNA (L^+/D) = 2.2. d_{DNA} is seen to expand from 24.5 Å to 57.1 Å. The solid line through the data is the prediction of a packing calculation where the DNA chains form a space-filling 1D lattice. **(b)** Schematic drawing of DNA–membrane multilayers, showing the increase in distance between DNA chains as the membrane charge density is decreased (i.e. as Φ_{DOPC} increases) at the isoelectric point. Adapted from [12–14].

which was measured to be 3.4 nm, consistent with the pitch of B-DNA [32,33].

Thus, the CL–DNA complex is self-assembled into a new 'hybrid' phase of matter, namely a 2D smectic phase of DNA chains coupled to a 3D smectic phase of lipid bilayers. On length scales larger than the finite-sized lattice of DNA chains, dislocations produce a 2D nematic phase of chains [27,28]. The DNA–lipid condensation can be understood to occur as a result of the release of 'bound' counterions in solution. In solution, the distance along the DNA chain between two negative charges (from the phosphate groups) is equal to b_o = 1.7 Å. This is substantially less than the Bjerrum length in water, b_j = 7.1 Å, which corresponds to the distance at which the Coulomb energy between two unit charges is equal to the thermal energy, k_BT. A nonlinear Poisson–Boltzmann analysis shows that counterions will condense on the DNA backbone until the Manning parameter, $\xi = b_j/b'$, approaches 1 [34]. (b' is the renormalized distance between negative charges after counterion condensation.) A similar analysis shows that counterions also condense near the surface of 2D membranes (i.e. within the Gouy–Chapman layer) [35]. Through DNA–lipid condensation, the cationic lipid tends to fully neutralize the phosphate groups on the DNA, in effect replacing and releasing the originally condensed counterions in solution. Thus, the driving force for higher-order self-assembly is the release of counterions, which were one-dimensionally bound to DNA and two-dimensionally bound to cationic membranes, into solution.

The inverted hexagonal H_{II}^C phase of CL–DNA complexes

A commonly used charge-neutral lipid in CL–DNA mixtures is di-oleoyl phosphatidylethanolamine (DOPE). It is empirically known that transfection efficiency in mammalian cells is typically improved using CL–DNA complexes that contain DOPE instead of DOPC as the helper-lipid [36]. Recent XRD shows that DOPE-containing complexes may give rise to a completely different columnar inverted hexagonal H_{II}^C liquid-crystalline structure (Figure 5) [16].

Figure 6 shows SAXS scans of positively charged CL–DNA complexes for DOTAP/DNA (wt/wt) = 3 as a function of increasing Φ_{DOPE} (weight fraction of DOPE) in the DOPE/DOTAP CL mixtures [16]. The internal structure of the complex changes completely with increasing

Figure 4

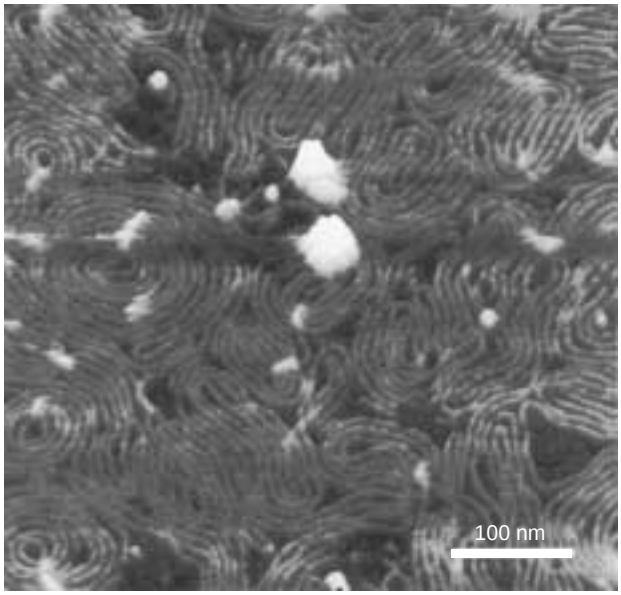

High-resolution AFM image of plasmid DNA adsorbed on a cationic bilayer (DPTAP) coating a freshly cleaved mica surface. The highly packed DNA chains are clearly visible. The measured width of the DNA is 2 nm, which is close to the diameter of B-DNA. Adapted from [32]. See also [33].

Figure 5

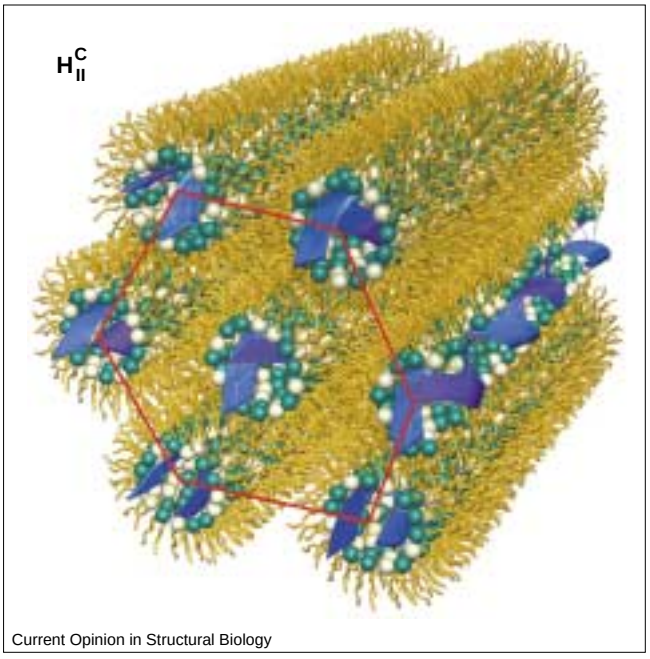

Schematic of the inverted hexagonal H_{II}^{C} phase (cylinders consisting of DNA coated with a lipid monolayer arranged on a hexagonal lattice) of CL–DNA complexes.

Figure 6

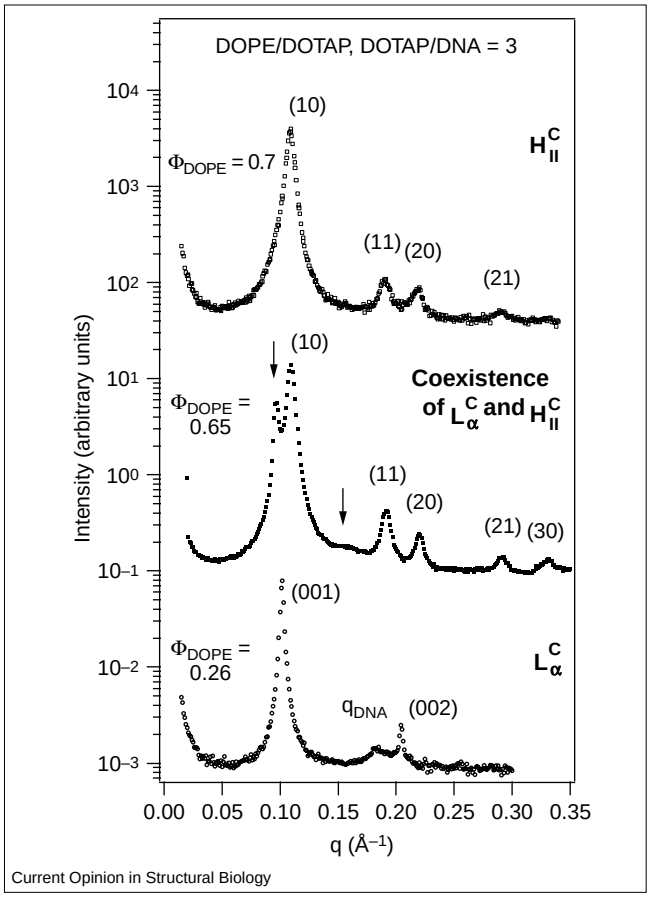

Synchrotron SAXS patterns of the lamellar L_{α}^{C} and columnar inverted hexagonal H_{II}^{C} phases of positively charged CL–DNA complexes as a function of increasing weight fraction of DOPE, Φ_{DOPE}. At Φ_{DOPE} = 0.26, the SAXS scan results from a single phase with the lamellar L_{α}^{C} structure shown in Figure 1. At Φ_{DOPE} = 0.7, the SAXS scan results from a single phase with the columnar inverted hexagonal H_{II}^{C} structure shown in Figure 5. At Φ_{DOPE} = 0.65, the SAXS scan shows coexistence of the L_{α}^{C} (arrows) and H_{II}^{C} phases. Adapted from [16].

DOPE/DOTAP ratios. SAXS data of complexes with Φ_{DOPE} = 0.26 and 0.70 clearly show the presence of two different structures. At Φ_{DOPE} = 0.26, SAXS of the lamellar L_{α}^{C} complex shows sharp peaks at q_{001} = 0.099 Å^{-1} and q_{002} = 0.198 Å^{-1}, resulting from the lamellar periodic structure (d = $2\pi/q_{001}$ = 63.47 Å) with DNA intercalated between cationic lipid, analogous to the structure in DOPC/DOTAP–DNA complexes (Figure 1).

For 0.7 < Φ_{DOPE} < 0.85, the peaks of the SAXS scans of the CL–DNA complexes are indexed perfectly on a 2D hexagonal lattice with a unit cell spacing of a = $4\pi/[(3)^{0.5}q_{10}]$ = 67.4 Å for Φ_{DOPE} = 0.7. Figure 6 at Φ_{DOPE} = 0.7 shows the first four order Bragg peaks of this hexagonal structure at q_{10} = 0.107 Å^{-1}, q_{11} = 0.185 Å^{-1}, q_{20} = 0.214 Å^{-1} and q_{21} = 0.283 Å^{-1}. Thus, the structure is consistent with a 2D columnar inverted hexagonal structure in which the DNA molecules are surrounded by a lipid monolayer, with the DNA–lipid inverted cylindrical micelles arranged on a hexagonal lattice (Figure 5). The structure resembles that of the inverted hexagonal H_{II} phase of pure DOPE in excess water [37], with the water space inside the lipid micelle filled by DNA. Again assuming an average lipid monolayer thickness of 20 Å, the diameter of the micellar void in the H_{II}^{C} phase is close to 28 Å, again sufficient for a DNA molecule with approximately two hydration shells. For Φ_{DOPE} = 0.65, the L_{α}^{C} and H_{II}^{C} structures coexist, as shown in Figure 6 (arrows point to the [001] and q_{DNA} peaks of the L_{α}^{C} phase), and are nearly epitaxially matched, with a ≈ d. For Φ_{DOPE} > 0.85, the H_{II}^{C} phase coexists with the H_{II} phase of pure DOPE, which has peaks at q_{10} = 0.0975 Å^{-1}, q_{11} = 0.169 Å^{-1}, q_{20} = 0.195 Å^{-1}, with a unit cell spacing of a = 74.41 Å.

The interplay between lamellar L_{α}^{C} and hexagonal H_{II}^{C} phases of CL–DNA complexes

In order to understand the stability of the lamellar and hexagonal phases, we consider the interplay between the electrostatic and membrane elastic interactions in the CL–DNA complexes; this interplay is expected to determine the different structures. Recent theoretical work suggests that electrostatic interactions alone are expected to favor the inverted hexagonal H_{II}^{C} phase over the lamellar L_{α}^{C} phase, which minimizes the charge separation between the anionic groups on the DNA chain and the cationic lipids [22,23]. However, the electrostatic interaction may be resisted by the membrane elastic cost (per unit area), F/A = 0.5 κ $(1/R–1/R_o)^2$, of forming a

cylindrical monolayer membrane around DNA. Here, κ is the lipid monolayer bending rigidity, R is the actual radius and R_o is the natural radius of curvature of the monolayer. Many lipids (e.g. phosphatidylcholine, phosphatidylserine, phosphotidylglycerol, cardiolipin) have a cylindrical shape, with the head group area approximately equal to the hydrophobic tail area, and tend to self-assemble into lamellar structures with a natural curvature $C_o = 1/R_o = 0$. Other lipids (e.g. phosphatidylethanolamine) have a cone shape, with a smaller head group area than tail area, and give rise to a negative natural curvature $C_o < 0$. Alternatively, lipids with a larger head group area than tail area have $C_o > 0$.

It is well appreciated [38] that, in many lipid systems, the 'shape' of the molecule that determines the natural curvature of the membrane, $C_o = 1/R_o$, will also determine the actual curvature, $C = 1/R$, which describes the structure of the lipid self assembly (e.g. $C = 0 \rightarrow$ lamellar L_α; $C_o < 0 \rightarrow$ inverted hexagonal H_{II}; $C_o > 0 \rightarrow$ hexagonal H_I). This is particularly true if the bending rigidity of the membrane is large ($\kappa/k_BT >> 1$), because then a significant deviation of C from C_o would cost too much elastic energy. However, if the bending cost is low, with $\kappa \approx k_BT$, then C may deviate from C_o without costing much elastic energy, especially if another energy is lowered in the process. Here I present experimental data pertaining to both situations: first, situations in which the bending rigidity is large and the structure of the self assembly is controlled by the 'shape' of the molecule (described in the next paragraph); second, situations in which κ is lowered enough that C deviates from C_o because of the electrostatic energy favoring a different curvature and structure.

We can understand the L_α^C to H_{II}^C transition as a function of increasing Φ_{DOPE} by noting that, in contrast to the helper-lipid DOPC and the cationic lipid DOTAP, which have a zero natural curvature ($C_o^{DOTAP,DOPC} = 1/R_o^{DOTAP,DOPC} = 0$), DOPE is cone-shaped, with $C_o^{DOPE} = 1/R_o^{DOPE} < 0$. Thus, the natural curvature of the monolayer mixture of DOTAP and DOPE is driven negative, with $C_o = 1/R_o = \Phi_{DOPE}\, C_o^{DOPE}$. Hence, as a function of increasing Φ_{DOPE}, we expect a transition from the L_α^C to the H_{II}^C phase, as observed experimentally, that is now expected to be favored by the elastic free energy. Thus, the helper-lipid DOPE induces the L_α^C to H_{II}^C transition by controlling the spontaneous radius of curvature R_o of the lipid layers.

The L_α^C to H_{II}^C transition was recently observed to occur along a different path by reducing the bending rigidity κ of the lipid layer [16]. The reduction of κ along this pathway reduces the membrane elastic energy, which otherwise prevents the formation of the H_{II}^C phase, which is favored by electrostatics. In these experiments, a new class of helper-lipid molecule was used, consisting of DOPC mixed with the membrane-soluble cosurfactant molecule hexanol [16]. Although cosurfactant molecules, which typically consist of long-chain alcohols (e.g. pentanol, hexanol), are not able to stabilize an interface separating hydrophobic and hydrophilic regions, when mixed with longer chain 'true' surfactants, they are known to lead to dramatic changes in interface elasticities. Simple compressional models of surfactant chains show that the bending rigidity of membranes (κ) scales with chain length, l_n ($l_n \propto \delta_m$, where n is the number of carbons per chain), and the area per lipid chain, A_L, as $\kappa \propto l_n^4 / A_L^5$ [39]. The mixing of cosurfactants with lipids is expected to lead to both a thinner membrane and a larger area per chain, and results in a strong suppression of κ, making the membrane highly flexible. Experimental studies have shown that the addition of cosurfactants such as pentanol to membranes of lamellar phases with a mole ratio of between two and four leads to a significant decrease in κ from about 20 k_BT to about 2–5 k_BT [40].

DNA condensation on membrane surfaces

Aside from the biomedical gene delivery applications of CL–DNA complexes, the lamellar L_α^C phase (Figure 1) affords an ideal *in vitro* model system to explore the nature of DNA–DNA interactions and DNA compaction on a surface. The existence of distinct states of DNA compaction is, of course, vital to the functions of viruses, bacteria and eucaryotic cells. The more compact states enable the efficient packing of genomic DNA within the small confines of the eukaryotic nucleus, the bacterial cytoplasm and viral capsids. Equally important are the less compact states of DNA required during much of the life cycle to allow proteins access to the DNA template for a multitude of biological tasks (e.g. gene regulation, transcription, replication). The biologically relevant DNA-condensing agents *in vivo* include cationic proteins (e.g. histones) and polyamines, such as spermidine and spermine, with sufficiently high valence ($Z \geq 3$) [41]. In bacteria, polyamine molecules such as spermine (+4) and spermidine (+3) are known to be critical to DNA compaction [41]. There have been a number of theoretical [42] and experimental studies aimed at elucidating the fundamental physical mechanisms responsible for DNA condensation. Experimental studies done *in vitro* have found that DNA condensation from bulk solution is critically dependent on the valence of the counterion and that a valence of three or more is required in order to overcome the inherently large electrostatic repulsive barrier between the like-charged polyelectrolytes [18]. Furthermore, experiments show that counterions with $Z = 2$ simply screen the electrostatic repulsions, but do not lead to DNA collapse.

The spatial dimension available to DNA plays a key role in the interactions between chains. DNA chains adsorbed onto a cationic membrane are found to undergo a collapse transition in the presence of simple divalent cationic biological salts, such as Ca^{2+}, Mg^{2+} and Mn^{2+}. Synchrotron XRD shows that the collapsed phase consists of DNA chains electrostatically tethered by divalent counterions in

Figure 7

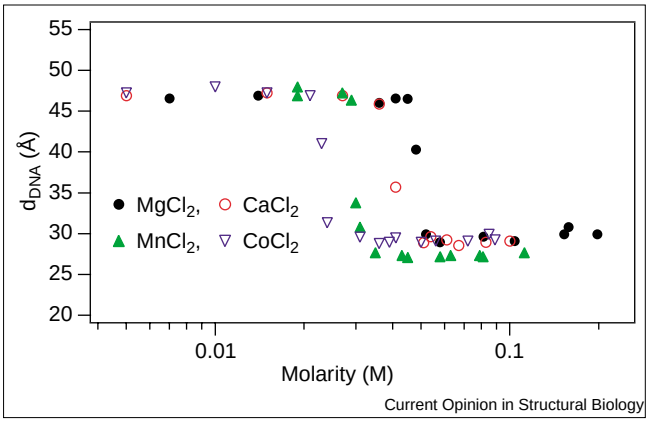

Variation of the DNA–DNA spacing, d_{DNA}, of the L_α^C complex with increasing concentrations of four different divalent salts. The sharp transition between uncondensed and condensed phases of DNA is evident. See text for further details. Adapted from [43].

2D [43]. This is seen in Figure 7, which is a plot of the variation $d_{DNA}(M)$ for four different divalent cations. In the uncondensed phase, the DNA spacing, which is fixed at $d_{DNA} = 47 \pm 0.5$ Å ($\Phi_{DOPC} = 0.6$), remains constant independent of the ion type until a critical salt concentration, M*. Above M*, the 1D lattice of DNA chains condenses to a state in which the surfaces of DNA chains are separated by a distance on the order of the divalent cation diameter. This distance ($d_{DNA} = 29 \pm 0.4$ Å) is independent of the ionic species, with the exception of Mn^{2+}, which causes condensation to $d_{DNA} = 27.3$ Å, which is about 2 Å smaller than the other divalent ions. The trapped counterions form a novel 1D liquid between the chains at a density of 0.63 ions/DNA base pair. Thus, with increasing divalent salt concentration M, the L_α^C complexes undergo a transition between the two states depicted in Figure 8. At low salt concentrations, M < M*, the DNA spacing is set by the membrane charge density and the divalent salt ions diffuse freely within the complex (Figure 8 left). At a critical salt concentration, M = M*, the surface-confined DNA undergoes a sharp transition into a state with DNA helices separated by the ionic diameter of the divalent ions (Figure 8 right). This state represents the most compact state of DNA on a surface *in vitro* and suggests applications in the high-density storage of genetic information and organometallic materials processing.

These observations suggest that simple divalent electrolytes may play a critical role in controlling the extent of compaction of genomic nucleic acid, for example, in rod-shaped viruses, in which the genome is adsorbed onto a curved cationic protein-based surface. Furthermore, the observed enhanced counterion-mediated attractive forces leading to DNA condensation for Z = 2 in 2D may act between any like-charged macromolecules, such as cytoskeletal fibers or charged polypeptides adsorbed onto or near surfaces *in vivo*.

Figure 8

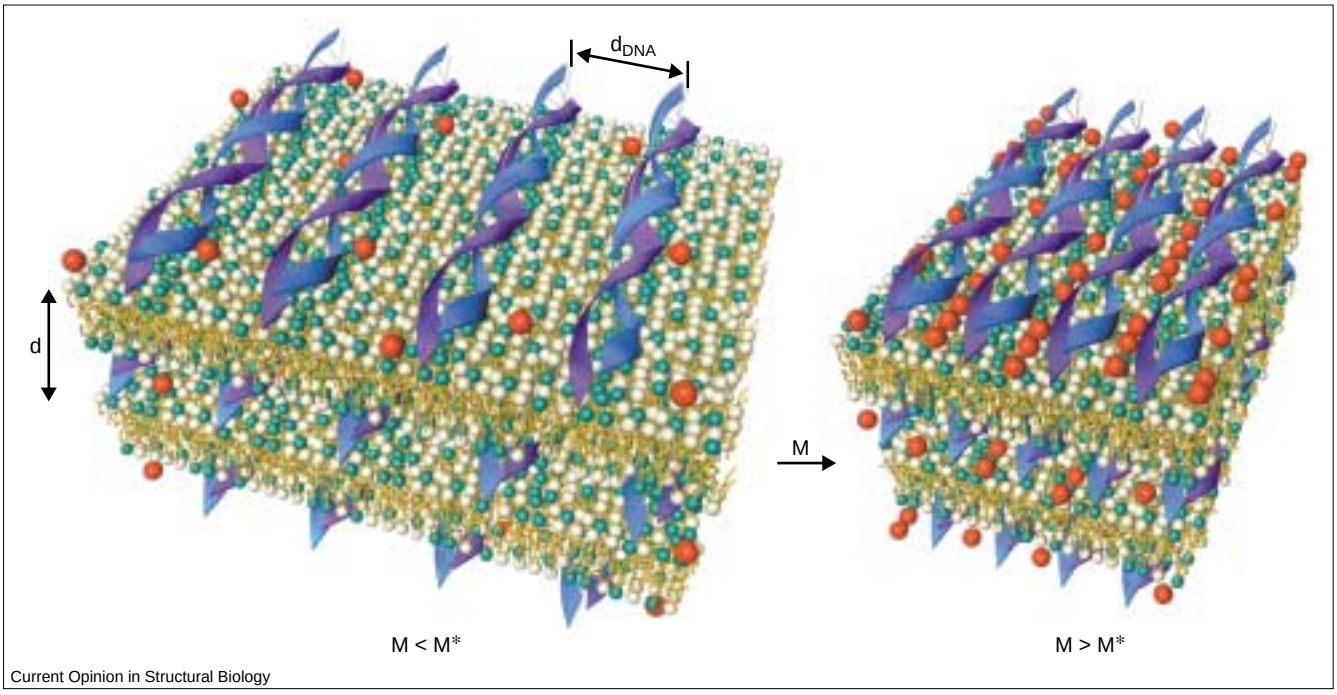

Schematic illustration of the L_α^C complex structure variation during the DNA condensation transition in 2D. During the transition, the spacing between the DNA double helices rapidly decreases to a separation on the order of the diameter of the condensing ions (shown as red spheres). M is the molar concentration of the condensing ions. M* is the value of the molar concentration at which the DNA condensation transition occurs.

Future directions

A major goal of research on CL–DNA complexes is to elucidate the key parameters resulting in the different CL–DNA complex structures and to establish the correlation between the different structures and transfection efficiency. It is known that transfection efficiency, mediated by mixtures of cationic lipids and neutral 'helper-lipids', varies widely and unpredictably. The choice of helper-lipid has been empirically established to be important; for example, many papers report that transfection is believed to be significantly more efficient in mixtures of the cationic lipid DOTAP and the neutral helper-lipid DOPE than in mixtures of DOTAP and the similar helper-lipid DOPC. From XRD work, we know that DOTAP/DOPC–λ-DNA complexes form the multilamellar L_{α}^{C} structure (Figure 1). The work described in this review shows that DOTAP/DOPE–λ-DNA complexes may also form the distinctly different self-assembled inverted hexagonal H_{II}^{C} structure.

The data represent one example of a correlation between the self-assembled structure of CL–DNA complexes and the transfection efficiency of this particular concentration regime in DOTAP/DOPE and DOTAP/DOPC complexes: the empirically established, more transfectant DOPE-containing complexes in mammalian cell culture exhibit the H_{II}^{C} structure, rather than the L_{α}^{C} structure found in DOPC-containing complexes. What makes the H_{II}^{C} structure more transfectant than the L_{α}^{C} structure? Recent fluorescent optical microscopy in cell culture medium for both a high transfectant complex (DOTAP/DOPE, 72% DOPE) and a low transfectant complex (DOTAP/DOPC, 72% DOPC) shows two distinct interactions between these two types of complexes and mouse fibroblast L-cells [44]. The images reveal a most likely origin for why the different structures transfect cells with varying efficiency: in contrast to L_{α}^{C} complexes, which remain stable inside cells, H_{II}^{C} complexes show fusion of their lipids with the mouse cell membranes (e.g. endosomal and plasma membranes), which results in DNA release. I caution that I believe that highly transfectant L_{α}^{C} complexes may be designed in certain concentration regimes.

Clearly, much work remains before we have a complete understanding of the various possible self-assembled structures of CL–DNA complexes and an understanding, at the molecular and self-assembled levels, of all of the critical parameters that control the different structures. Even more work will be required to relate the structures to biological function, namely, the interactions of CL–DNA complexes with cellular components inside animal cells that lead to gene release and expression. For example, recent work that studied the interactions between CLs and filamentous actin (an abundant anionic cell protein) *in vitro* showed that CL–filamentous actin complexes may spontaneously assemble into multilamellar tubules [45]. Thus, actin may remove CLs from CL–DNA complexes and facilitate DNA release from complexes in cells *in vivo*.

The broad, long-term objective of this research is to develop a fundamental science base that will lead to the design and synthesis of optimal nonviral carriers of DNA for gene therapy and disease control. Simultaneously, a major long-term objective is to improve the efficiency of delivering large pieces of DNA containing important human genes and their regulatory sequences (> 100 kbp), which, at present, can only be achieved with synthetic vectors. The structure/function data obtained from the research should allow us to begin the formidable task of the rational design of these self assemblies for enhanced gene delivery applications from the ground up, beginning with the chemical structure of the lipids and the correct compositions of mixtures, including the functional plasmid.

Acknowledgements

I gratefully acknowledge the contributions of my graduate students and postdoctorals past and present, in particular, Ilya Koltover, Alison Lin, Nelle Slack, Ayesha Ahmad, Heather Evans, Kai Ewert, Uwe Schulze, Joachim Raedler, Tim Salditt, Thomas Pfohl and Gerard Wong. I would also like to acknowledge my collaborators, Hans Werner Schmidt, Youli Li, Cyril George and Charles Samuel. I have benefited enormously through extensive discussions with Fyl Pincus, Robin Bruinsma, Tom Lubensky, Bill Gelbart and Avinoam Ben-Shaul. Supported by National Institutes of Health R01 GM59288 and the National Science Foundation DMR-9972246. Also supported by a University of California Biotechnology Research and Education Program Training Grant 99-14 and a Los Alamos-UC collaborative grant CULAR STB-UC:99-216. The synchrotron X-ray experiments were carried out at the Stanford Synchrotron Radiation Laboratory, supported by the US DOE. The Materials Research Laboratory at Santa Barbara is supported by NSF-DMR-0080034.

References and recommended reading

Papers of particular interest, published within the annual period of review, have been highlighted as:

- • of special interest
- •• of outstanding interest

1. Li S, Huang L: Nonviral gene therapy: promises and challenges. *Gene Ther* 2000, 7:31-34.

2. •• Chesnoy S, Huang L: Structure and function of lipid-DNA complexes for gene delivery. *Annu Rev Biophys Biomol Struct* 2000, 29:27-47.

This is an excellent comprehensive review that summarizes much of the work going on worldwide on synthetic delivery systems designed for gene therapy applications, including work in the biotechnology sectors, as well as clinical studies.

3. Clark PR, Hersh EM: Cationic lipid mediated gene transfer: current concepts. *Curr Opin Mol Ther* 1999, 1:158-176.

4. Miller AD: Cationic liposomes for gene therapy. *Angew Chem Int Edn Engl* 1998, 37:1768-1785.

5. Felgner PL, Gadek TR, Holm M, Roman R, Chan HW, Wenz M, Northrop JP, Ringold GM, Danielsen M: Lipofection: a highly efficient, lipid-mediated DNA-transfection procedure. *Proc Natl Acad Sci USA* 1987, 84:7413-7417.

6. Zhu N, Liggitt D, Liu Y, Debs R: Systemic gene expression after intravenous DNA delivery into adult mice. *Science* 1993, 261:209-211.

7. Wolff JA (Ed): *Gene Therapeutics: Methods and Applications of Direct Gene Transfer.* Boston: Birkhauser; 1994.

8. Nabel GJ, Nabel EG, Yang ZY, Fox BA, Plautz GE, Gao X, Huang L, Shu S, Gordon D, Chang AE: Direct gene transfer with DNA liposome complexes in melanoma – expression, biologic activity, and lack of toxicity in humans. *Proc Natl Acad Sci USA* 1993, 90:11307-11311.

9. Harrington JJ, Bokkelen GV, Mays RW, Gustashaw K, Willard HF: Formation of ***de novo*** centromeres and construction of first-generation human artificial microchromosomes. *Nat Genet* 1997, 15:345-355.

10. Willard HF: Artificial chromosomes coming to life. *Science* 2000, • 290:1308-1309.
Willard summarizes and brings the reader up to date with new developments on producing and using human artificial chromosomes. The paper emphasizes applications to gene delivery/therapy and human genetics.

11. Friedmann T: Overcoming obstacles to gene therapy. *Sci Am* 1997, 276:96-101.

12. Raedler JO, Koltover I, Salditt T, Safinya CR: Structure of DNA-cationic liposome complexes: DNA intercalation in multi-lamellar membranes in distinct interhelical packing regimes. *Science* 1997, 275:810-814.

13. Salditt T, Koltover I, Radler JO, Safinya CR: Two-dimensional smectic ordering of linear DNA chains in self-assembled DNA-cationic liposome mixtures. *Phys Rev Lett* 1997, 79:2582-2585.

14. Koltover I, Salditt T, Safinya CR: Phase diagram, stability and overcharging of lamellar cationic lipid–DNA self assembled complexes. *Biophys J* 1999, 77:915-924.

15. Salditt T, Koltover I, Raedler JO, Safinya CR: Self-assembled DNA-cationic lipid complexes: two-dimensional smectic ordering, correlations, and interactions. *Phys Rev E* 1998, 58:889-904.

16. Koltover I, Salditt T, Raedler JO, Safinya CR: An inverted hexagonal phase of DNA-cationic liposome complexes related to DNA release and delivery. *Science* 1998, 281:78-81.

17. Lasic DD, Strey HH, Stuart MCA, Podgornik R, Frederik PM: The structure of DNA-liposome complexes. *J Am Chem Soc* 1997, 119:832-833.

18. Bloomfield VA: Condensation of DNA by multivalent cations: considerations on mechanisms. *Biopolymers* 1991, 44:269-282.

19. Livolant F, Leforestier A: Condensed phases of DNA: structures and phase transitions. *Prog Poly Sci* 1996, 21:1115-1164.

20. Gustafsson J, Arvidson G, Karlsson G, Almgren M: Complexes between cationic liposomes and DNA visualized by cryo-TEM. *Biochim Biophys Acta* 1995, 1235:305-312.

21. Sternberg B, Sorgi FL, Huang L: New structures in complex formation between DNA and cationic liposomes visualized by freeze-fracture electron microscopy. *FEBS Lett* 1994, 356:361-366.

22. May S, Ben-Shaul A: DNA-lipid complexes: stability of honeycomb-like and spaghetti-like structures. *Biophys J* 1997, 73:2427-2440.

23. Dan N: The structure of DNA complexes with cationic liposomes — cylindrical or flat bilayers? *Biochim Biophys Acta* 1998, 1369:34-38.

24. Bruinsma R: Electrostatics of DNA cationic lipid complexes: isoelectric instability. *Eur Phys J B* 1998, 4:75-88.

25. Bruinsma R, Mashl J: Long-range electrostatic interaction in DNA cationic lipid complexes. *Europhys Lett* 1998, 41:165-170.

26. Harries D, May S, Gelbart WM, Ben-Shaul A: Structure, stability, and thermodynamics of lamellar DNA-lipid complexes. *Biophys J* 1998, 75:159-173.

27. O'Hern CS, Lubensky TC: Sliding columnar phase of DNA lipid complexes. *Phys Rev Lett* 1998, 80:4345-4348.

28. Golubovic L, Golubovic M: Fluctuations of quasi-two-dimensional smectics intercalated between membranes in multilamellar phases of DNA cationic lipid complexes. *Phys Rev Lett* 1998, 80:4341-4344.

29. Roux D, Safinya CR: A synchrotron x-ray study of competing undulation and electrostatic interlayer interactions in fluid multimembrane lyotropic phases. *J Phys France* 1988, 49:307-318.

30. Safinya CR: Rigid and fluctuating surfaces: a series of synchrotron X-ray scattering studies of interacting stacked membranes. In *Phase Transitions in Soft Condensed Matter*. Edited by Riste T, Sherrington D. *Nato ASI Series B* 1989, 211:249-270.

31. Podgornik R, Rau DC, Parsegian VA: Parametrization of direct and soft steric-undulatory forces between DNA double helical polyelectrolytes in solutions of several different anions and cations. *Biophys J* 1994, 66:962-971.

32. Mou J, Czajkowsky DM, Zhang Y, Shao Z: High-resolution atomic-force microscopy of DNA: the pitch of the double helix. *FEBS Lett* 1995, 371:279-282.

33. Fang Y, Yang J: Two-dimensional condensation of DNA molecules on cationic lipid membranes. *J Phys Chem B* 1997, 101:441-449.

34. Manning GS: Limiting laws and counterion condensation in polyelectrolyte solutions. I. Colligative properties. *J Chem Phys* 1969, 51:924-933.

35. Zimm BH, Bret ML: Counter-ion condensation and system dimensionality. *J Biomol Struct Dyn* 1983, 1:461-471.

36. Farhood H, Serbina N, Huang L: The role of dioleoyl phospatidylethanolamine in cationic liposome mediated gene therapy. *Biochim Biophys Acta* 1995, 1235:289-295.

37. Seddon JM: Structure of the inverted hexagonal phase and non-lamellar phase transitions of lipids. *Biochim Biophys Acta* 1989, 1031:1-69.

38. Israelachvili JN: *Intermolecular and Surface Forces*, edn 2. London: Academic Press; 1992.

39. Szleifer I, Ben-Shaul A, Gelbart WM: Chain packing statistics and thermodynamics of amphiphile monolayers. *J Phys Chem* 1990, 94:5081-5089.

40. Safinya CR, Sirota EB, Roux D, Smith GS: Universality in interacting membranes: the effect of cosurfactants on the interfacial rigidity. *Phys Rev Lett* 1989, 62:1134-1137.

41. Lewin B: *Genes VI*. Oxford: Oxford University Press; 1997.

42. Gronbech-Jensen N, Mashl RJ, Bruinsma RF, Gelbart WM: Counterion-induced attraction between rigid polyelectrolytes. *Phys Rev Lett* 1999, 78:2477-2480.

43. Koltover I, Wagner K, Safinya CR: DNA condensation in two dimensions. *Proc Natl Acad Sci USA* 2000, 97:14046-14051.

44. Lin AJ, Slack NL, Ahmad A, Koltover I, George CX, Samuel CE, Safinya CR: Structure-function studies of lipid-DNA nonviral gene delivery systems. *J Drug Target* 2000, 8:13-27.

45. Wong GCL, Tang JX, Lin A, Li Y, Janmey PA, Safinya CR: Hierarchical self-assembly of F-actin and cationic lipid complexes: stacked three-layer tubule networks. *Science* 2000, 288:2035-2039.